CENTENNIAL FEATURE ARTICLE

Development of Ultrafast Photochromic Organometallics and Photoinduced Linkage Isomerization of Arene Chromium Carbonyl Derivatives[†]

Tung T. To[‡] and Edwin J. Heilweil*

Optical Technology Division, Physics Laboratory, National Institute of Standards and Technology, Gaithersburg, Maryland 20899-8443

Charles B. Duke III, Kristie R. Ruddick, Charles Edwin Webster,* and Theodore J. Burkey*

Department of Chemistry, 213 Smith Chemistry Building, The University of Memphis, Memphis, Tennessee 38152-3550

Received: August 1, 2008; Revised Manuscript Received: December 24, 2008

We review recent studies of processes relevant to photoinduced linkage isomerization of organometallic systems with the goal of preparing organometallics with an efficient and ultrafast photochromic response. The organometallic system thus corresponds to two linkage isomers with different electronic environments that are responsible for different optical properties. Much of this work has focused on examining processes following irradiation of cyclopentadienyl manganese tricarbonyl derivatives (compounds **3**−**21**) including solvent coordination, thermal relaxation, solvent displacement by tethered functional groups (chelation), dissociation of tethered functional groups, and linkage isomerization. A new platform is investigated for obtaining a photochromic response in new experiments with arene chromium dicarbonyl complexes. A photochromic response is observed for arene chromium dicarbonyl complexes with tethered pyridine and olefin functional groups based on light-driven linkage isomerization on the nanosecond time scale. Irradiation at 532 nm of **23** ($[Cr\{\eta^6\text{-}C_6H_5CH(2\text{-}Py\text{-}\kappa N)CH_2CH=CH_2\}(CO)_2]$) (Py = pyridine) results in the isomerization to **22** ($[Cr\{\eta^6\text{-}C_6H_5CH(2\text{-}Py)CH_2\text{-}\eta^2\text{-}CH=CH_2\}(CO)_2]$), and 355 nm irradiation isomerizes **22** to **23**. The ultrafast linkage isomerization has been investigated at room temperature in *n*-heptane solution on the picosecond to microsecond time scale with UV- or visible-pump and IR-probe transient absorption spectroscopy by comparing the dynamics with model compounds containing only a tethered pyridine. Irradiation of **24** ($[Cr\{\eta^6\text{-}C_6H_5(CH_2)_3(2\text{-}Py)\}(CO)_3]$) and **25** ($[Cr\{\eta^6\text{-}C_6H_5(CH_2)_2(2\text{-}Py)\}(CO)_3]$) at 289 nm induces CO loss to immediately yield a Cr−heptane solvent coordinated intermediate of the unsaturated Cr fragment, which then converts to the κN^1-pyridine chelate within 200 and 100 ns, respectively. Irradiation of **26** ($[Cr\{\eta^6\text{-}C_6H_5CH_2(2\text{-}Py)\}(CO)_3]$) also induces CO loss to immediately yield three species: the Cr−heptane solvent coordinated intermediate, a κN^1-Py nitrogen chelate, and an agostic η^2-chelate in which the pyridine is coordinated to the metal center via a C−H agostic bond as opposed to the nitrogen lone pair. Both the transient Cr−heptane coordinated intermediate and the agostic pyridine chelate convert to the stable κN^1-pyridine chelate within 50 ns. Similar reaction dynamics and transient species are observed for the chelate **33** ($[Cr\{\eta^6\text{-}C_6H_5CH_2(2\text{-}Py)\text{-}\kappa N\}(CO)_2]$) where a Cr−Py bond, not a Cr−CO bond, initially cleaves.

Background and Previous Studies

Our interest in photochromic organometallics evolved from early photoacoustic calorimetry (Burkey) and transient infrared spectroscopy (Heilweil) investigations of the energetics and dynamics of organometallics. Both techniques require relatively high quantum yields to observe transient intermediates, and this requirement led to the study of compounds that have high quantum yields. Many metal carbonyls not only fit this requirement but also have large IR absorption making them amenable to time-resolved infrared (TRIR) studies. The results of several investigators over the years made it clear that the yield-determining steps for photosubstitution were occurring on a subpicosecond time scale.[1] The photolysis of $Cr(CO)_6$ is prototypical of many metal carbonyls (Scheme 1). The 16-electron metal center of $Cr(CO)_5$ is coordinatively unsaturated, and so reactive that it stereospecifically bonds to virtually any species including argon and possibly neon.[2] Alkanes form σ-complexes with bond energies around 10 kcal/mol.[3] As a result, for any solvent as reactive as an alkane, the second step is essentially irreversible because the diffusion of CO is faster than displacement of the coordinated solvent. $Cr(CO)_5(solv)$ is

* Corresponding authors. E-mail: E.J.H., edwin.heilweil@nist.gov; C.E.W., cewebstr@memphis.edu; T.J.B., tburkey@memphis.edu.
‡ NIST Guest Researcher/Postdoctoral Research Associate.

Centennial Feature Article

J. Phys. Chem. A, Vol. 113, No. 12, 2009 **2667**

Tung T. To: Staff Scientist, Arizona Chemical Asia Ltd. Singapore. Regional Office 51, Goldhill Plaza, Savannah, Georgia 1201 W. Lathrop Ave, Savannah, GA 31415. Research Associate, National Institute of Standards and Technology, Physics Laboratory: Edwin Heilweil, advisor. Ph.D. (2005) The University of Memphis, Memphis, TN: Ted Burkey, Advisor. Research includes organometallic photochemistry, molecular switches, and organic syntheses.

Edwin J. Heilweil: Staff Research Chemist, Optical Technology Division, Physics Laboratory, National Institute of Standards and Technology, Gaithersburg, MD 20899-8443 (1985—present). NRC Postdoctoral Research Fellow, National Bureau of Standards (1984—1985), John Stephenson, advisor; Ph.D. (1983) Chemistry Department, University of Pennsylvania, Philadelphia, PA; Robin Hochstrasser, advisor. B.A./M.A. (1978) Chemistry and Mathematics, Brandeis University, Waltham, MA. Research includes ultrafast spectroscopy of vibrational energy transfer and photochemistry; surface dynamics; solar energy materials; terahertz spectroscopy of biomolecules; and terahertz imaging for homeland security.

Charles B. Duke III: Ph.D. Candidate, The University of Memphis, Department of Chemistry, Memphis, TN: Ted Burkey, Advisor. Currently Postdoctoral Research Associate, University of Tennessee Health Sciences Center, Pharmaceutical Sciences Department, Memphis, TN: Duane Miller, advisor. Research interests include organometallic photochemistry, organic synthesis, and X-ray crystallography.

Kristie R. Ruddick: Graduate Student, The University of Memphis, Department of Chemistry, Charles Edwin Webster, Advisor. M.S., University of Arizona: Dennis L. Lichtenberger, Advisor. Research includes computational chemistry, inorganic chemistry, and organometallic synthesis.

Charles Edwin Webster: Assistant Professor, The University of Memphis, Department of Chemistry. Past positions include Visiting Professor, Zhengzhou University, Department of Chemistry; Research Scientist, Texas A&M University; Lecturer, Texas A&M University. Post doctoral fellow, Texas A&M University: Michael B. Hall, Advisor and Ph.D. (1999), Department of Chemistry, University of Florida: Russell S. Drago, Michael C. Zerner, and Michael J. Scott, Advisors. Research includes studies of inorganic, bioinorganic, and organometallic chemistry; structure and bonding; and homogeneous and heterogeneous catalysis.

Theodore J. Burkey: First Tennessee Professor, The University of Memphis, Department of Chemistry, Tennessee. Postdoctoral fellow, LSU Baton Rouge: William Pryor, Advisor Research Associate, National Research Council Canada, Ottawa, Ontario: David Griller, Advisor and Ph.D. (1982), Department of Chemistry, UC San Diego: Robert Fahey. Research includes organic synthesis, organometallics, ultrafast photochromic materials, and photochemistry.
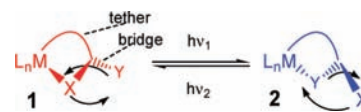
SCHEME 1

SCHEME 2

completely converted to product when a dispersed ligand (L) is in excess of all other solutes. Thus, the product-determining step is dependent on two competing cage reactions: CO recombination and solvent addition. Both of these cage processes ultimately reduce the quantum yield as well as the overall rate of substitution.

With the goal to expand our studies to other compounds, we became acutely interested in the factors that affect the ultrafast processes that control product formation. Thus, to increase the quantum yield, either the efficiency of the cage processes must be reduced or that of substitution must be increased. We reasoned that a substitution that competes on the same timescale as a cage process would ultimately do both, and our goal became very simple: make the substitution faster than any other process. Logically, L must be in the cage to compete with a cage process, requiring that L either be the solvent or be at very high concentration. However, quantum yield studies demonstrate that even these conditions are not sufficient. For example, the quantum yield for substitution of $Cr(CO)_6$ in benzene or acetonitrile was the same as in cyclohexane.[4] On the other hand, the quantum yield does decrease with increasing viscosity and supports the idea that a slower diffusing solvent molecule does not compete as well with CO recombination.[4] Clearly geminate recombination with a reactive metal would not be eliminated by a diffusive process, and the addition of a ligand must be
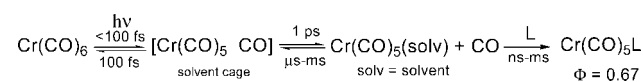
coupled with the photodissociation. An idealized coupling mechanism based on a linkage isomerization is depicted in Scheme 2. Schematically we imagined that the dissociation of X would create a torque about a tether that would rotate Y to the metal before recombination of X or solvent addition could occur. L_n represents one or more ligands that are not necessarily the same and confer important electronic, structural, and physical properties but are otherwise inert. These ideas led to our fascination with the development of an ultrafast molecular device based on a reversible linkage isomerization driven by light; however, selectivity in driving the reaction to one or the other isomer would require that the isomers have different chromophores. Thus began our interest in designing, synthesizing and characterizing bistable, photochromic materials.[5]

A photochrome[6] is any pair of compounds that interconvert via a photochromic response. In addition to high quantum yields, important properties include low fatigue (no side reactions) and good spectral resolution of chromophores. Robust photochromes are most often based on reversible unimolecular processes (such as an isomerization) that avoid the diffusive loss of a critical component.[7–11] Organic-based systems typically rely on reversible electrocyclic ring formation,[12] but because of the inherent asymmetry of the forward and reverse reactions, factors that favor ring formation disfavor the ring opening and vice versa. For example, ring opening typically has a more favorable entropy. The linkage isomerization in Scheme 2 is essentially a ligand substitution, but it is also the interconversion of two chelates where ring formation and opening occurs in both directions. Regardless of conformation or bond energy differences between the isomers, there must be a significant thermal barrier between **1** and **2** (Scheme 2) for both isomers to be stable. This barrier is bypassed by the photochromic pathways.

The exchange of functional groups X and Y during the linkage isomerization of Scheme 2 is functionally equivalent to a ligand substitution. The potential advantages of the photochrome in Scheme 2 are better understood when compared with a purely bimolecular photochromic system based on a ligand substitution mechanism (Scheme 3). The lifetimes are based on typical results reported in the literature.[1,3b,c,13] Compared to a cage complex, M(solv) will have an extended lifetime allowing it time to (a) recombine with L_1 effectively lowering the quantum yield, (b) react with starting material or other species that may lead to fatigue, or (c) react with L_2 for the desired photochromic response. The same model applies to the reverse photoreaction; therefore, M(solv) is a common intermediate for both directions. Even if $M-L_1$ and $M-L_2$ both form M(solv) with unit quantum yield, this common intermediate will partition between $M-L_1$ and $M-L_2$ as products such that the quantum yield for the forward and reverse directions combined can be no better than 1. Thus, any modifications to improve the yield in one direction will reduce the yield in the reverse direction and at best the average yield will be 0.5.

Unit quantum yields in both directions can be obtained if a common intermediate is avoided; i.e., the photochemical reaction

2668 *J. Phys. Chem. A, Vol. 113, No. 12, 2009*

To et al.
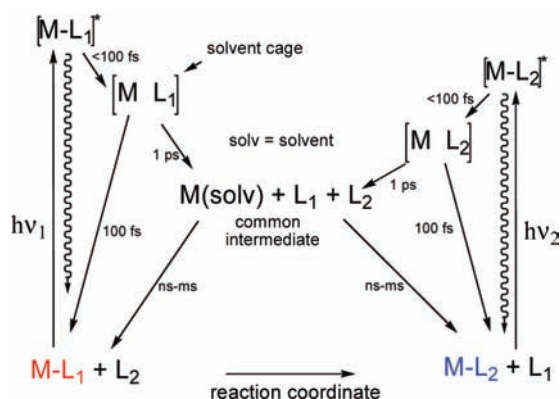
SCHEME 3

SCHEME 4

surfaces do not cross. With respect to Scheme 3, species like $[ML_1]$, $[ML_2]$, and M(solv) must be completely avoided. A reaction coordinate is defined not only by the atomic positions and electronic state but also by the velocity (direction and speed) of the atoms. Thus, irradiation of **1** and **2** could lead to a species with identical positions and electronic states, but until they begin to thermally equilibrate, their ultrafast dynamics are different because the directions of rotation are opposite. **1** and **2** will interconvert if the rotations are not interrupted. In general, this requires the rotation to be faster than processes that might otherwise interfere with the rotation. From an energetic point of view, there can be no significant potential well in the reaction coordinate, i.e., no restoring force that reverses the course of the reaction. For a linkage isomerization (like that in Scheme 2) the most likely restoring force would be a collision with a solvent molecule that would result in recombination. The estimated collision frequency at room temperature is approximately 10^{13}, and only a small fraction of these collisions are likely to have the correct trajectory and energy to impede the linkage isomerization. The photochrome idealized in Scheme 2 should have two related features: (1) minimum rotation for linkage isomerization to optimize the rate and (2) the position of Y in **1** (and X in **2**) to minimize intervention of solvent or other species that could interfere with the reaction. The positioning of Y for **1** close to the metal center avoids M−X recombination via a concerted motion of X and Y whereby Y immediately coordinates following dissociation of X and before X or Y has a collision that can cause recombination. Furthermore, the proximity of Y to the reactive metal center excludes intervening solvent molecules and hence precludes ultrafast solvent coordination. The same condition must be met for the reverse reaction if near unit quantum yields and ultrafast reaction rates are to be realized for a reversible reaction.

The quantum yields will not be high, regardless of the positions of X and Y in **1** and **2**, if the excited states deactivate before dissociation. Wrighton and Giordano demonstrated for CpMn(CO)$_2$L that L can have a dramatic effect on the quantum yield of the dissociation of L.[14] Yields are high (0.65) for L = CO and low (0.14) for L = piperidine. The initial excited-state population is expected to be a metal-to-ligand charge transfer state that crosses over to a dissociative manifold, most likely an excited ligand field state.[15] Thus, low yields likely correlate with the poor overlap of excited states; however, there needs to be further investigation of this and other factors such as cage recombination and multiplicity.[16]

In addition to high quantum yields, good spectral resolution of **1** and **2**, thermal stability of MX and MY bonds, and low fatigue are desirable properties. There are many variables that could affect the performance of the photochrome depicted in
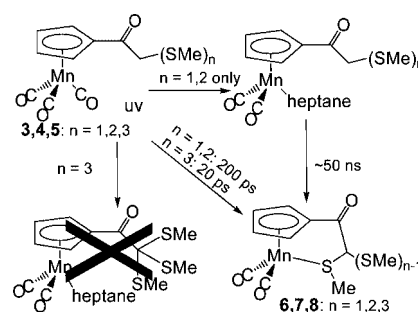
Scheme 2: the choice of (1) functional groups X and Y, (2) the bridge between X and Y, (3) the tether structure, (4) the metal center, (5) the spectator ligands, and (6) the solvent. These variables are likely to affect more than one property including the chromophore absorption wavelength, the lifetime of the excited state, coordination of solvent, and the recombination of X or Y. In addition, they will play a role in the thermal stability of M−X and M−Y bonds as well as the photolability of **1** and **2**. Thus it will be challenging to optimize all the desirable properties in a single photochrome. For example, X and Y that provide good spectral resolution in **1** and **2** may not make strong bonds with the metal or may not be easily positioned near the metal center for a fast linkage isomerization. Large aromatic groups that favor long wavelength absorption for better spectral resolution are more likely to have collisions that impede fast linkage isomerization. Changing X and Y could result in an excited state that has an efficient deactivation pathway that would limit the initial dissociation of X or Y. Strain or rigidity in the tether could alter the M−X bond energy, the ease of photodissociation of X as well as the wavelength of the metal-centered chromophore. From a different but related perspective, several fundamental processes are recognizable during a linkage isomerization including ligand substitution, chelation, dechelation (ring opening), solvent coordination, vibrational relaxation, and electronic interconversion and relaxation. Many if not all of the enumerated variables can affect each of these processes; therefore, understanding each of these processes in detail is vital to designing successful photochromes. To understand the effects of the variables on these processes, several model systems have been prepared and studied. The results have led to development of more advanced models and photochromes.

Photochelation of (Cp^R)Mn(CO)$_3$ (Cp^R = C$_5$H$_4$R) Complexes with Pendant Sulfides. One of our first goals was to establish that a pendant functional group could trap a metal center on the picosecond or faster time scale and increase the photosubstitution yield relative to the bimolecular substitution. Early studies used (Cp)Mn(CO)$_3$ derivatives because they are thermally stable, have intrinsically high quantum yields, and are synthetically accessible. Equally important, all reports to date indicate that irradiation of CpMn(CO)$_2$L leads only to dissociation of L in the condensed phase as long as M−L has a weaker bond than M−CO.[14,17,18] The quantum yield for CO photosubstitution on CpMn(CO)$_3$ without a side chain was reported to be 0.65 ± 0.10 at 313 nm.[14] For those side-chain conformations of **3** (Scheme 4) where the sulfur is not near the metal, previous studies of ring formation indicate a conformational "walk" leading to ring formation occurs in about 100 ps for five- to six-membered rings.[19] This process is too slow to compete with cage recombination of CO, which is expected to be similar to that of CO with M(CO)$_5$ (<300 fs).[20] On the other hand, about half the time the side chain of **3** is expected to

Centennial Feature Article

J. Phys. Chem. A, Vol. 113, No. 12, 2009 **2669**

have conformations with the sulfur near the metal without intervening solvent. Thus, the side-chain sulfur has an opportunity to compete with solvent coordination and CO recombination, and we expected an incremental increase in the quantum yield for CO substitution with a pendant functional group. Instead, a unit quantum yield was observed, indicating no CO recombination occurred.[18] This report was the first example of a unit quantum yield for an organometallic ligand substitution and demonstrated that cage recombination could be eliminated. These results were in contrast to those reported earlier by Yang et al. where the yield was less than one and independent of ring size for bis-phosphine complexes $CpMn(CO)_2(Me_2P(CH_2)_nPMe_2)$ ($n = 1-3$) were irradiated to form four- to six-membered rings [quantum yield = $(0.60-0.62) \pm 0.06$], and the yield was also the same as that for CO substitution of $CpMn(CO)_2(PPh_3)$ with PPh_3 (quantum yield = 0.59 ± 0.05).[17,21]

Time-resolved infrared (TRIR) studies of **3**–**5** revealed that ultrafast chelation was not solely responsible for the lack of CO recombination and a unit quantum yield.[22] For mono- or bis-pendant sulfides (**3** and **4**, Scheme 4) both an alkane coordinated intermediate and a chelate formed in nearly equal amounts within the 30 ps resolution of the experiments (limited by thermal relaxation of the CO vibrations following excitation); however, the solvent was displaced ultimately by a pendant sulfide on a much longer timescale. Like the monosulfide **3**, calculations of the side-chain conformations indicated that a sulfur atom was near the metal center 50% of time for the bis-sulfide, consistent with the initial product distribution. On the other hand, a sulfur is always near the metal for three pendant sulfide species (**5**): TRIR revealed only chelate formation with no solvent-coordinated intermediate. This system is the first example where ultrafast solvent coordination was eliminated during ligand substitution.

Exclusion of Reactive Solvent Coordination During Photochelation of $(Cp^R)Mn(CO)_3$ Complexes with Pendant Sulfides. The application of photochromic organometallics in the solid state may require the use of polymers with functional groups that could potentially coordinate to the metal center. Thus, the design of a system that could undergo chelation and ultimately linkage isomerization without intervention by matrix functional groups would be desirable. We hypothesized that the exclusion of solvent coordination following irradiation of the tris-sulfide **5** was due to the accessibility of sulfur and not blocking of the solvent from the metal because solvent has access to the opposite side of the metal. We reasoned that both solvent and sulfide can encounter the metal on the subpicosecond time scale, but the weaker metal alkane bond could not fully form a σ-bond at the thermally excited metal center and thus allowed the more stable (steeper energy gradient) metal–sulfur bond to form.

We tested this hypothesis by irradiating **3**–**5** in acetonitrile, which is known to form a stable Mn–nitrile coordinate bond.[23] Both steady-state irradiation and TRIR studies demonstrated that all three chelates **6**–**8** were generated without the formation of acetonitrile coordinated product (Scheme 5). The origin of this preference is believed to be a solvent effect that favors a conformation with the sulfur near the metal center. The question remains, why does solvent not add from the other side of the metal? One possibility is that there is a precoordination of the sulfur to the metal or a weak sulfur–carbonyl interaction that preorganizes the sulfide, yet no spectroscopic evidence for such an interaction has been observed.
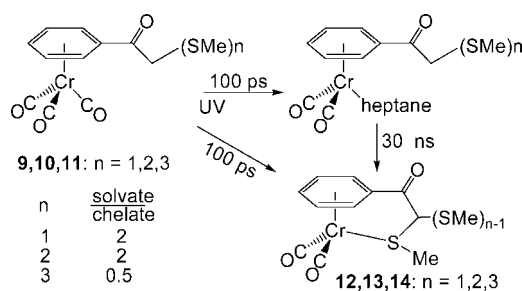
SCHEME 5
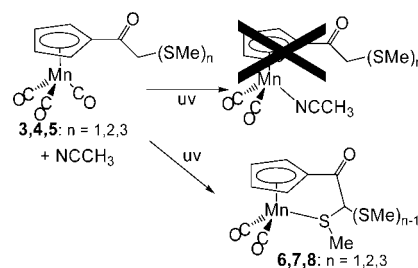
SCHEME 6
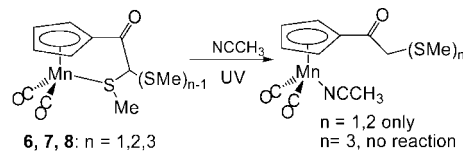
An alternative explanation for the lack of acetonitrile adduct in steady-state or picosecond TRIR experiments is that this species is unstable to displacement by a sulfide group. This explanation seemed unlikely because nitrile derivatives such as $(CpR)Mn(CO)_2(RCN)$ are known to be thermally stable,[24] although the chelates **6**–**8** may have some ring strain. Furthermore, heptane displacement was found to occur on the nanosecond time scale and acetonitrile coordinates more strongly to the metal; thus, acetonitrile coordination should be easily detected by TRIR if not in steady-state irradiation experiments. These issues were ultimately put to rest by preparing the acetonitrile adducts in the presence of a sulfide side chain.

The tris-sulfide **5** was a good candidate to establish if it is possible to eliminate ultrafast coordination of a polymer matrix functional group during chelation. By analogy to the TRIR studies of **3**–**5** in acetonitrile, a polyacrylonitrile film containing homogeneously dispersed **5** was studied.[25] In both FTIR and picosecond TRIR experiments, chelate was formed exclusively and no nitrile coordinated complex was observed.

Photolytic Ring Opening of $(Cp^R)Mn(CO)_2$ Sulfide Chelates in Acetonitrile. Steady-state irradiation of chelates **6**–**8** in acetonitrile under the same conditions of photochelation revealed that the mono- and bis-sulfides formed stable acetonitrile coordinated products whereas the tris-sulfide did not (Scheme 6).[23] We can conclude that **3**–**5** do form chelates without any transient acetonitrile coordination. The lack of acetonitrile coordinated product following irradiation of the tris-sulfide **8** is very interesting. Because the chromophores and bond energies must be nearly identical for all three chelates **6**–**8**, we concluded that the tris-sulfide undergoes sulfide dissociation immediately followed by recombination before acetonitrile addition could occur. However, we suspect that the recombination is actually a linkage isomerization and not simply the recombination of the dissociated sulfur. The coordinated sulfur is not in the plane of the side-chain carbonyl; therefore, the photodissociation impulse should rotate the tris-sulfide group (similar to Scheme 2), delivering a different sulfide to the metal. This study was the first known example of a linkage isomerization with tethered functional groups without competition from ultrafast solvent coordination.

Comparison of $ArCr(CO)_3$ Derivatives with Pendant Sulfides. To design efficient photochromes, we needed to understand what features were responsible for the high yields and ultrafast dynamics of CpMn complexes. Thus we investigated analogous ArCr complexes (Scheme 7)[26] where the di- and tricarbonyl derivatives are known to have high (but not unit)
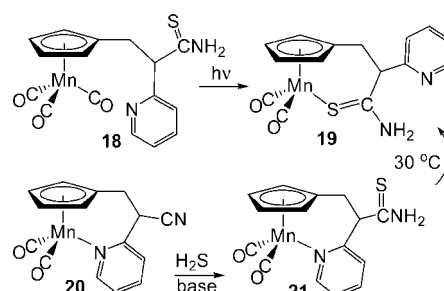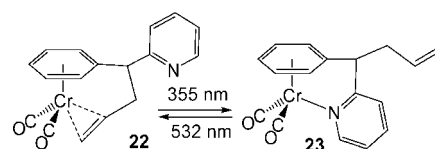
SCHEME 7

SCHEME 8
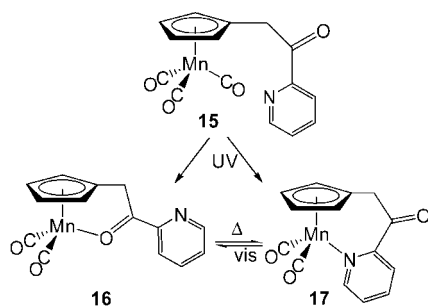
quantum yields.[27] In contrast to results for the CpMn series (Scheme 4), heptane coordinated intermediates and chelates were observed in each case following irradiation in heptane. Notably, the tris-sulfide **11** formed substantial heptane coordinated intermediates within 100 ps unlike the Mn tris-sulfide **8**. Within 30 ns the heptane coordinated intermediate converted to chelates **12−14**; however, attempts to prepare the chelates via steady-state photolysis were not successful. Although results in THF were similar to those for heptane, in acetonitrile the results were dramatically different than for **3−5**: only acetonitrile coordinated intermediates were observed and no chelates. Nonchelated sulfides are not labile, and the difference between manganese and chromium reactivity is attributed at least partially to ring strain and the greater distance between chromium and sulfur at their closest conformational approach.

Photochromic Cp^RMn Complex Based on a Bifunctional Tether. Clearly two different side-chain functional groups are needed to create a photochrome. We began investigating different functional groups with the study of **15** (Scheme 8). Although O-coordination of carbonyl groups generally did not lead to stable complexes, the effect of chelation was not known. Irradiation of **15** (Scheme 8) produced **16**, one of few examples of a CpMn(CO)$_2$ derivative with a blue chromophore, thus making available the "primary colors" (yellow and red (Cp)Mn(CO)$_2$L complexes had been prepared previously).[28] It was found that **16** preferentially forms but thermally rearranges in a few minutes at room temperature to the pyridine chelate **17**. Visible irradiation isomerizes **17** to **16** followed by thermal isomerization back to **17**. DFT calculations accurately predicted activation parameters for the O-to-N linkage isomerization that were subsequently confirmed by variable temperature NMR kinetic studies ($\Delta H^{\ddagger} = 21$ kcal/mol and $\Delta S^{\ddagger} = 4$ eu). These results indicated that the activation enthalpy needs to increase by only 4−5 kcal to make **16** kinetically stable. An important finding from our calculations (and supported by the small activation enthalpy) was that the thermal linkage isomerization was not dissociative; rather, the metal "walked" along the π system from O to N via an η^2 pyridine intermediate. Evidence for an η^2-agostic intermediate has also been implicated in our TRIR and computational studies of ArCr(CO)$_3$ chelation (vide infra).

SCHEME 9

SCHEME 10

A parallel study provided evidence that a bridged functional group that otherwise forms a stable metal−ligand bond can be labile.[28] Irradiation of **18** (Scheme 9) produced the thioamide chelate without evidence of pyridine chelation. We demonstrated that a pyridine chelate with an identical side chain (**20**), save the substitution of the thioamide by a nitrile, is stable and can be isolated following photolysis of the parent tricarbonyl. No nitrile chelate was observed in spite of the fact that nitriles normally form stable ligands with CpMn(CO)$_2$.[29] This result was anticipated because it has been reported that nitrile chelates are unstable for 6-membered rings presumably due to the angle strain caused by the linear bonding preferred by the nitrile.[30] Thus, **21** should be thermodynamically stable. When **21** was prepared independently by a thermal method, it isomerized to **19** during isolation. The evidence indicates that the linkage isomers are in an equilibrium favoring the thioamide chelate, but the barrier for isomerization is low between **21** and **19**; therefore, the pyridine chelate is not normally observed. The bridge thus provides a low energy "conduit" for isomerization and the pyridine chelate may in general be kinetically labile if its linkage isomer is thermodynamically more stable. These findings suggest important conditions for designing bistable photochromes.

Photochromic Arene Chromium Carbonyl with Pendant Alkene and Pyridine. In this paper, we report the first example of a bistable photochromic organometallic based on the linkage isomerization of arene chromium complexes with tethered alkene and pyridine groups (**22** ([Cr{η^6-C$_6$H$_5$CH(2-Py)CH$_2$-η^2-CH=CH$_2$}(CO)$_2$]) and **23** ([Cr{η^6-C$_6$H$_5$CH(2-Py-κN)CH$_2$-CH=CH$_2$}(CO)$_2$]). The mechanisms for reversible linkage isomerization between **22** and **23** are elucidated by comparing the TRIR spectra with those observed for **24**, **25**, **26** ([Cr{η^6-C$_6$H$_5$(CH$_2$)$_n$(2-Py)}(CO)$_3$], $n = 3$, 2, and 1, respectively), and **33** ([Cr{η^6-C$_6$H$_5$CH$_2$(2-Py-κN)}(CO)$_2$]. The objectives were to develop a chromium photochrome and to determine to what extent other processes compete with the linkage isomerization for relatively independent functional groups.

The arene chromium linkage isomers **23** and **22** with pendant alkene and pyridine functional groups were found to have a photochromic response (Scheme 10).[31] UV irradiation of a heptane solution of **22** increases the absorbance at 500 nm that subsequently decreases upon visible irradiation (Figure 1). Both **23** and **22** absorb at 500 nm but the extinction coefficient for **23** is much larger. The optical change is not completely reversible as indicated by the loss of the isosbestic point and
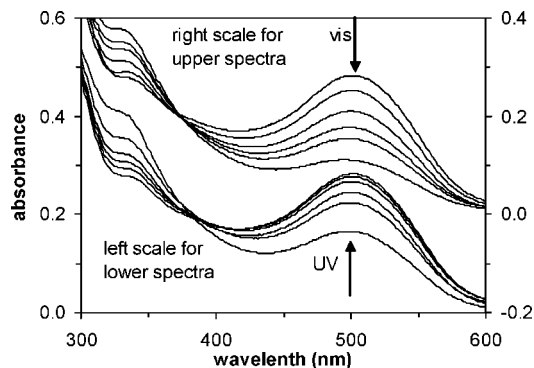
Centennial Feature Article

J. Phys. Chem. A, Vol. 113, No. 12, 2009 **2671**

Figure 1. UV−vis spectra of 2 mM **22** in heptane at room temperature during UV irradiation (lower spectra) and visible reaction (upper spectra). Lower spectra were recorded after a total of 0, 15, 30, 45, 60, and 90 s of UV irradiation. Upper spectra were recorded at additional 0, 30, 75, 135, 195, and 275 s of visible irradiation.
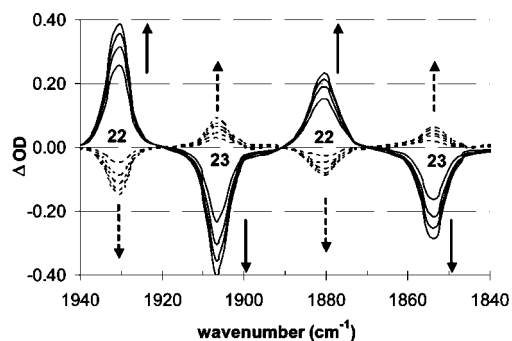

Figure 2. Reversible FTIR spectral changes upon 532 nm irradiation (solid arrows) of **23** in *n*-heptane forming **22** and subsequent 355 nm irradiation (dashed arrows) to regenerate **23**. The spectrum from the last 532 nm irradiation was subtracted from subsequent spectra with 355 nm irradiation. The sample was irradiated for 10 min between each spectral acquisition.

Figure 3. TRIR difference spectra acquired after 289 nm pulsed laser irradiation of **24** in *n*-heptane at 298 K. The spectra are offset vertically by 0.04 OD units. The FTIR difference spectrum was obtained after steady-state irradiation with a Hg lamp.

SCHEME 11

superscript = n, tether length

the 500 nm absorption (275 s visible irradiation) that is less than the value before UV irradiation. Bleaches centered at 285 nm (not shown) and 510 nm are assigned to Cr → CO and Cr → Py MLCT (metal-to-ligand charge transfer) absorptions, respectively. The absorption centered at 330 nm is assigned to the Cr → olefin MLCT absorption.

FTIR spectra also reveal that **23** and **22** undergo a linkage isomerization during visible and UV irradiation (Figure 2). When difference spectra are obtained following 532 nm irradiation of **23**, bleaches occur at 1854 and 1907 cm^{-1} for the loss of **23** whereas new absorptions for **22** grow in at 1878 and 1930 cm^{-1} (solid arrows). Additional difference spectra, obtained by subtracting the last spectrum after 532 nm irradiation from subsequent spectra following 355 nm irradiation, reveals bleaching for the 1878 cm^{-1} and 1930 cm^{-1} peaks of **22** whereas the 1854 and 1907 cm^{-1} peaks of **23** grow in intensity (dash arrows). Complete recovery of **23** does not occur indicating side product formation during extended irradiation. Similar results are also observed while monitoring **23** and **22** by proton NMR spectroscopy. The results taken together support the conclusion that a linkage isomerization is responsible for the photochromic response.

Ultrafast Chelation of Side-Chain Pyridine. Several transients are observed in TRIR spectra following irradiation of **22** and **23**, and examination of model compounds **24**, **25**, and **26** greatly assists the identification of transients (Scheme 11). Each of these compounds has a pyridine ring tethered to the benzene ring with a 3, 2, or 1 carbon chain, respectively, but no tethered alkene. After 200 ns, UV irradiation leads to pyridine chelates
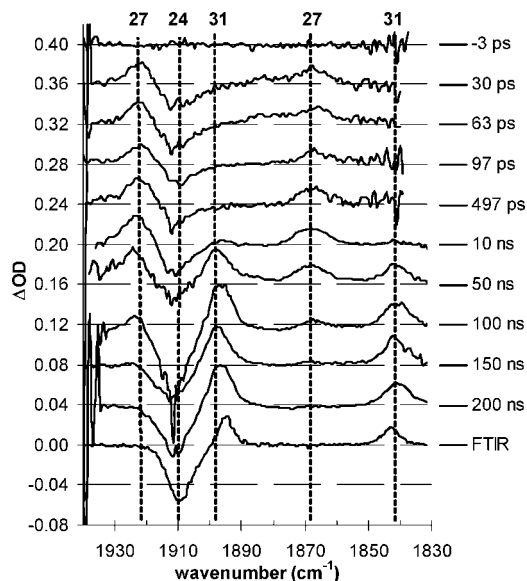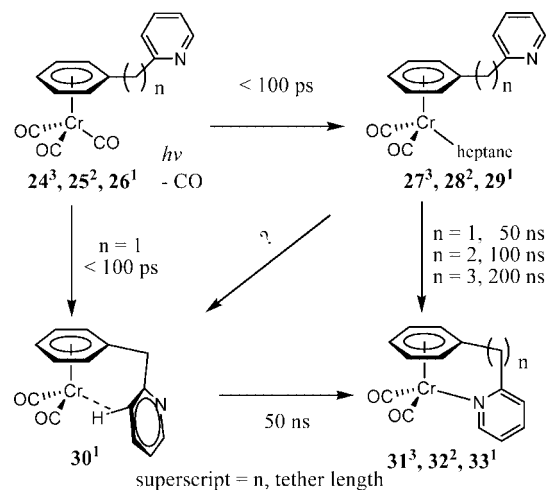
31, **32**, or **33**, respectively, where the structures have been independently confirmed by X-ray crystal structures, IR, and NMR spectroscopic methods.[31]

Prior to chelation, **24** (*n* = 3, Scheme 11) behaves the same as (η^6-benzene)Cr(CO)$_3$ with a free ligand in heptane.[32] UV irradiation induces CO loss from **24** to yield a Cr−heptane coordinated intermediate **27** as the only species observed within 100 ps. The loss of CO is indicated by a ground-state bleach of the metal CO-stretching peak near 1910 cm^{-1} (Figure 3). A second bleach feature of the tricarbonyl parent species occurring at 1979 cm^{-1} is not shown. A broad, red-shifted absorption feature occurring near 1880 cm^{-1} within 60 ps has been interpreted previously as arising from cooling of vibrationally hot product species.[33,34] Absorptions near 1867 and 1922 cm^{-1} appear within 100 ps and then decay within 200 ns. These two absorptions, which decay with indistinguishable kinetics (Figure S1, Supporting Information), suggest that they arise from a single transient. The assignment of the transient absorptions to the Cr−heptane coordinated intermediate **27** is consistent with those reported for (η^6-benzene)Cr(CO)$_2$(heptane) (1877 and 1927 cm^{-1}).[32] Finally, **27** decays as absorptions at 1842 and 1898 cm^{-1} grow (assigned to κN^1-Py chelate **31** based on
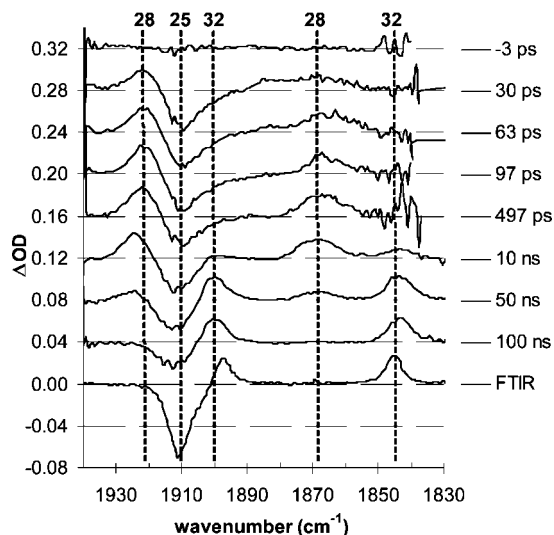
Figure 4. TRIR difference spectra acquired after 289 nm pulsed laser irradiation of **25** in *n*-heptane at 298 K. The spectra are offset vertically by 0.04 OD units. The FTIR difference spectrum was obtained after steady-state irradiation with a Hg lamp.

TABLE 1: Experimental and Computational Carbonyl Stretching Frequencies (cm^{-1}).

	experimental		computational		
complex	asym-metric	sym-metric	asym-metric	sym-metric	assigned coordination
22	1880	1930	1923	1959	C=C
23	1853	1907	1906	1940	N
34	1877	1922	1914	1945	agostic
35	1862	1922	1917	1951	solvent
24 ($n = 1$)	1910	1979	1945/1948	1998	CO
25 ($n = 2$)	1910		1931/1949	1996	CO
26 ($n = 3$)	1914		1944/1948	1997	CO
27 ($n = 3$)	1867	1922	1914	1950	solvent
28 ($n = 2$)	1868	1922	1910	1947	solvent
29/36 ($n = 1$)	1865	1922	1916	1951	solvent
29/37 ($n = 1$)	1865	1922	1917	1952	solvent
30 ($n = 1$)	1877	1922	1916	1947	agostic
31 ($n = 3$)	1842	1898	1895	1930	N
32 ($n = 2$)	1844	1900	1897	1931	N
33 ($n = 1$)	1852	1907	1904	1940	N

comparisons with genuine product). A dinuclear species is apparently inconsistent with the assignment for **31** because the bimolecular rate constant for the (η^6-C$_6$H$_6$)Cr(CO)$_2$(cyclohexane) with (η^6-C$_6$H$_6$)Cr(CO)$_3$ is 5 × 10^7 M^{-1} s^{-1}.[32] By analogy, the reaction of **27** with **24** would result in a 20 μs lifetime for 1 mM **24**. On the other hand, displacement of a coordinated solvent by a chelatable functional group has been reported to occur within 200 ns, which is consistent with our assignments (IR CO-stretch band assignments are listed in Table 1).[33,34]

Nearly identical results are observed for the irradiation of **25** (Figure 4, Scheme 11, $n = 2$) where the pyridine is tethered to the benzene ring with a two carbon chain. The heptane coordinated intermediate **28** (1867 and 1922 cm^{-1}) is also observed in less than 100 ps, but it decays more rapidly as the chelate **32** is formed within 100 ns (1840 and 1895 cm^{-1}).

The results are different for **26** (Figure 5, Scheme 11, $n = 1$) where the pyridine is tethered by a single carbon. After 100 ps, broad absorptions appear from 1850−1880 and 1922 cm^{-1}, which we attribute to spectral overlap of two species. The first transient is assigned to the solvent coordinated intermediate **29** (as observed for $n = 2$ and 3), which is again formed in less than 100 ps and decays in even less time (50 ns). The absorption peaks of the second transient are better observed in Figure 6 where **33** is irradiated instead of **26**.
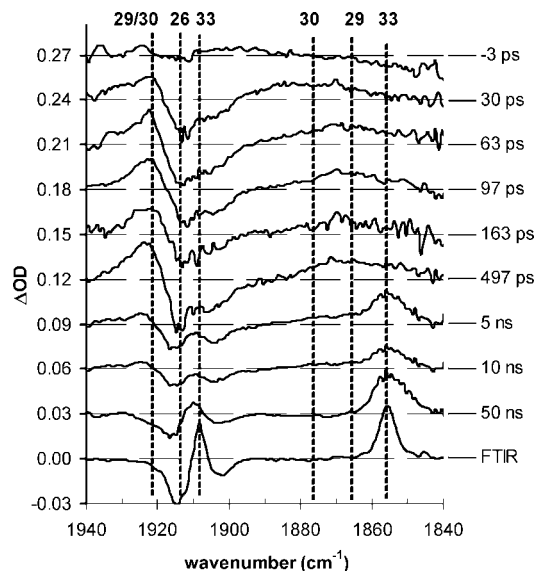

Figure 5. TRIR difference spectra acquired after 289 nm pulsed laser irradiation of **26** in *n*-heptane at 298 K. The spectra are offset vertically by 0.03 OD units. The FTIR difference spectrum was obtained after steady-state irradiation with a Hg lamp.
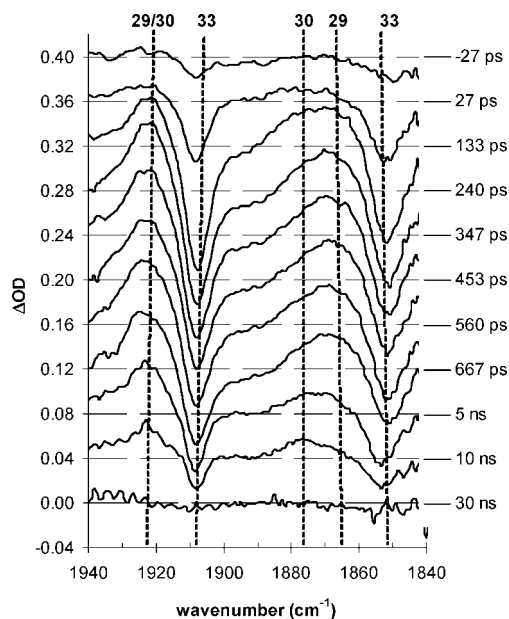

Figure 6. TRIR difference spectra acquired after 289 nm pulsed laser irradiation of **33** in *n*-heptane at 298 K. The spectra are offset vertically by 0.04 OD units.

The spectral changes for **33** ($n = 1$, dicarbonyl) are similar to those observed for **26** ($n = 1$, tricarbonyl) except that the CO-stretching peaks of **33** appear as two bleaches at 1852 and 1907 cm^{-1}, which completely recover because all transients decay to re-form **33**. The intensities near 1865 and 1880 cm^{-1} decay on different timescales (Figure S2, Supporting Information), which implies that there is more than one component under the broad absorption in this region. The transients having these CO-stretching frequencies cannot be a vibrationally hot species because of their relatively long lifetimes and they are blue-shifted from the parent species (rather than the expected red shift). One transient is tentatively assigned to **29** and the other transient to an agostic chelate **30**, in which the pyridine coordinates to the Cr metal center through a two-electron−three-center C−H agostic interaction and not via the nitrogen lone-pair (Scheme 11) (vide infra, for discussion of computed CO

Centennial Feature Article

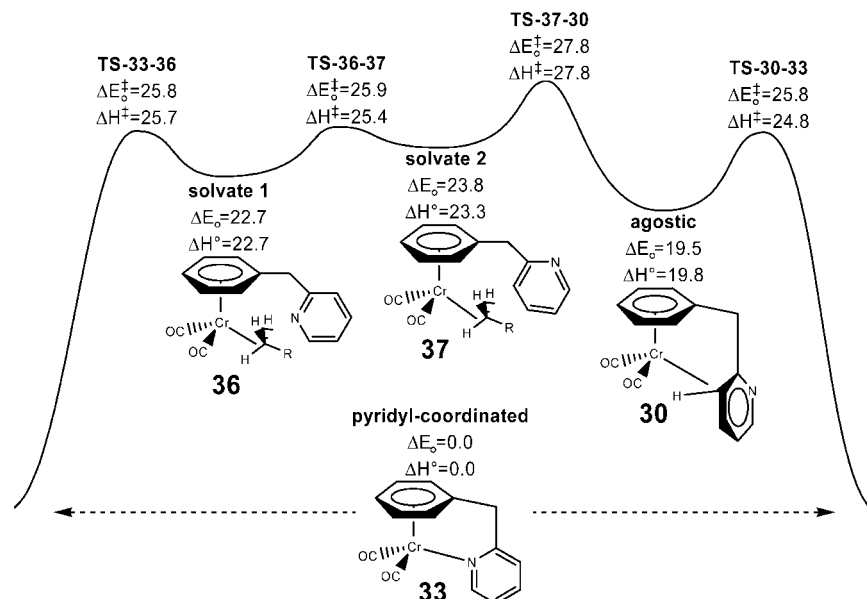*J. Phys. Chem. A, Vol. 113, No. 12, 2009* **2673**

Figure 7. Computationally derived potential energy surface showing formation and decay of solvate and agostic transient species.

frequencies). Though this agostic complex is a local minimum on the potential energy surface, a similarly structured η^2-π pyridyl structure is not a local minimum.[35] Both **29** and **30** appear in less than 100 ps and have nearly disappeared within 30 ns when the two bleaches of **33** have recovered. The computationally derived potential energy surface shown in Figure 7 illustrates three local minima (**36**, **37**, and **30**) corresponding to the two experimentally observed transients (**29** and **30**). Computational complexes **36** and **37** correspond to experimentally observed **29** and are solvent-coordinated isomers which differ only in the orientation of the pyridine ring. **TS-36−37** is a rotational transition state. **TS-37−30**, **TS-33−36**, and **TS-30−33** are best described as interchange transition states. **TS-37−30** is an exchange of two weakly bound ligands, σ-bound solvent and agostic CH. **TS-33−36** is the exchange of a weakly σ-bound solvent with an N-bound pyridyl group. **TS-30−33** is the exchange of a weakly bound agostic CH with an N-bound pyridyl group. As depicted, the enthalpy of activation ($\Delta H^{\ddagger}$) for conversion of solvent coordinated complex to the pyridine-coordinated complex (**36** → **33**) is 3.0 kcal/mol, and for the agostic species (**30** →**33**) $\Delta H^{\ddagger}$ is 5.0 kcal/mol. These low but significant activation enthalpies are consistent with the experimentally observed decays found in Figure 5. The assignments of the overlapping carbonyl stretching frequencies for the solvent-coordinated transients **29** and **30** are further substantiated by the results for computed CO frequencies for **36**, **37**, and **30** (listed in Table 1); i.e., **36** (1916/1951 cm^{-1}), **37** (1917/1952 cm^{-1}), and **30** (1916/1947 cm^{-1}) have overlapping CO frequencies.

Like other coordinatively unsaturated metal centers formed after CO photodissociation,[1] an (arene)Cr(CO)$_2$ fragment is expected to react immediately with the first species it encounters, which is normally the solvent or caged CO. The immediate formation of chelate from **26** but not from **24** or **25** suggests that only **26** has a conformation with the pyridine ring near the metal center when CO dissociates. It is even more interesting that only the agostic chelate **30** and not the η^1-σ chelate **33** is formed immediately from **26**, and it seems to suggest that the pyridine ring is in a conformation where the nitrogen is not nearby. No agostic chelates are observed for **24** or **25** at longer

delay times presumably due to a low barrier for rearrangement that can be attributed to a negligible ring strain in the transition state.

Comparing the spectra within the Cr series **24** to **26**, we note that the chain length of the pendant pyridine group does not affect the CO-stretching frequencies of the Cr−heptane solvent coordinated intermediates, but the CO-stretching frequencies of the Cr−Py chelates are monotonically blue-shifted as the chain length decreases (1842 and 1898 cm^{-1} for **31**, 1844 and 1900 cm^{-1} for **32**, and 1852 and 1907 cm^{-1} for **33**). Also note that the computed harmonic frequencies display the same blue-shift trend (1895 and 1930 cm^{-1} for **31**, 1897 and 1931 cm^{-1} for **32**, and 1904 and 1940 cm^{-1} for **33**). These observations further support our structural assignments of the observed transient species in which all the Cr−heptane solvent coordinated intermediates should have similar CO-stretching frequencies. The different chelate ring size and bond angles will result in different electronic interactions between the metal center and the tethered pyridine ligand which is consistent with the different CO-stretching peak frequencies.

TRIR Studies of a Reversible Linkage Isomerization. TRIR spectra were collected following irradiation of **23** on the picosecond, nanosecond, and microsecond timescales and are shown in Figures 8 and 9. Similar to the photobleaching of **33** in Figure 6, bleaches at 1852 and 1908 cm^{-1} are clearly apparent, indicating pyridine dissociation upon 532 nm irradiation of **23** in *n*-heptane. Likewise, broad absorptions are observed at higher frequencies from these parent bleaches. Ultimately, these features narrow and decay within 50 μs, leaving absorptions at 1880 and 1930 cm^{-1}, which correspond to the absorptions of **22** observed in steady-state FTIR spectra (Figure 2). Both a shoulder at 1862 cm^{-1} and the absorption at 1922 cm^{-1}, assigned to the solvent coordinated intermediate **35** (Scheme 12), decay within 50 ns, like that observed for the solvent coordinated intermediate following irradiation of **26** and **33**. A peak at 1877 cm^{-1} decays within 50 ns, revealing on its shoulder the 1880 cm^{-1} peak assigned to **22**. We attribute this decaying feature at 1877 cm^{-1} to the agostic pyridine chelate **34**. By analogy to **30**, a corresponding absorption should appear near 1922 cm^{-1}, coincident with the absorption of **35**. Because of the overlap with other absorptions in Figure 9 it is unclear
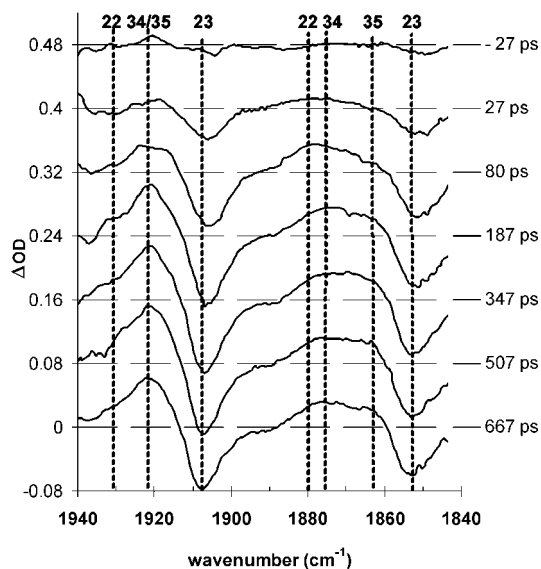
Figure 8. Picosecond TRIR difference spectra of **23** in *n*-heptane at 298 K acquired after 532 nm pulsed laser irradiation. The spectra are offset vertically by 0.08 OD units.

Figure 9. Nano/microsecond TRIR difference spectra of **23** in *n*-heptane at 298 K acquired after 532 nm pulsed laser irradiation. The spectra are offset vertically by 0.04 OD units.
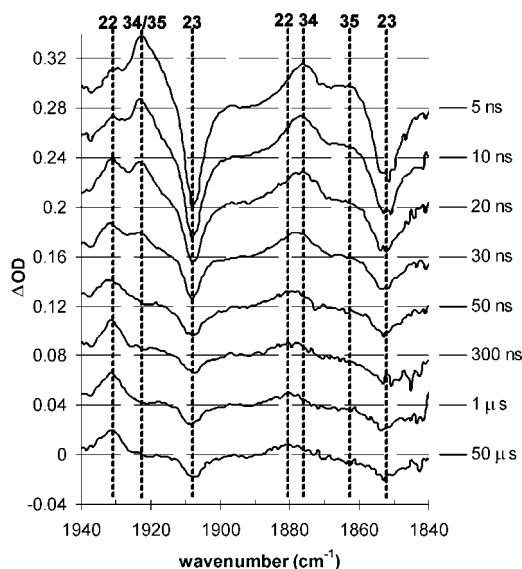

Figure 10. Picosecond and nanosecond switching dynamics showing **22** converting to **23** in *n*-heptane upon 355 nm irradiation.

SCHEME 12

the high degree of band overlap these complexes exhibit experimentally.

Summary and Conclusions

The arene chromium carbonyl complexes **23** and **22** with tethered pyridine and alkene groups are the first examples of a bistable, organometallic chromium photochrome. Ultrafast studies of the chelation for a series of model arene chromium carbonyl derivatives with a tethered pyridine group (**24**−**33**) and of the reversible linkage isomerization of **23** and **22** have been investigated on the picosecond to microsecond timescales. After photodissociation in each case of either CO or a tethered functional group, a heptane solvent coordinated intermediate is formed in less than 100 ps and converts within 200 ns to a stable κN^1 pyridine chelate and an η^2-π chelate in the case of **23** or **22**. Specifically, the linkage isomerization occurs 50 ns after irradiation of **23** or **22**. The formation of chelate occurs between 5 and 200 ns and is slower for longer side chains. Unlike the chelation observed after irradiation of cyclopentadienylmanganese derivatives with sulfide side chains,[18,22,23] no chelation was observed in less than a nanosecond except perhaps

whether **22** or **34** or both have formed before 1 ns. The absorptions at 1862 cm^{-1} along with that at 1922 cm^{-1} (**35**) disappear by 50 ns, and it appears that this transient along with **34** is converted into the starting material **23** because the bleaches at 1852 and 1908 cm^{-1} recover on this time scale whereas **22** apparently does not grow.

TRIR spectra were obtained for 355 nm irradiation of **22** (Figure 10). Bleaches of **22** at 1930 and 1880 cm^{-1} indicate alkene dissociation.[36] The growth of CO stretching peaks at 1853 and 1907 cm^{-1} for **23** does not begin until about 5 ns and is complete by 60 ns. Peaks for **35** appear near 1922 and 1862 cm^{-1} and decay by 60 ns. Due to poor spectral quality and overlap, we cannot conclude that there is picosecond isomerization of **22** to **23**. Similarly, spectral overlap makes it hard to determine whether **34** formed during this reaction. Computationally, **23**, **22**, **34**, and **35** were all found to be local minima on the potential energy surface. The computationally predicted infrared frequencies for these complexes (Table 1) corroborate
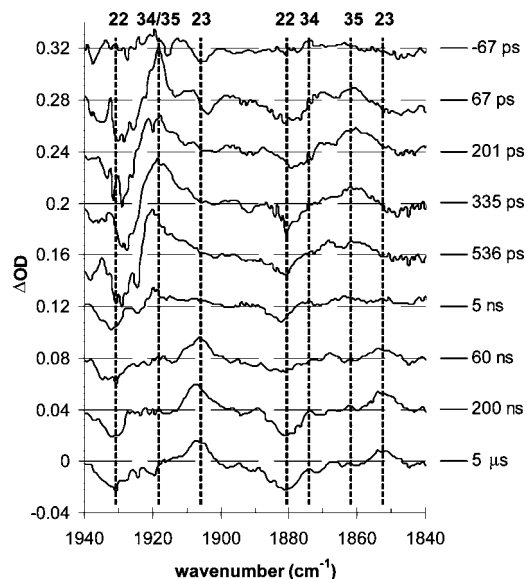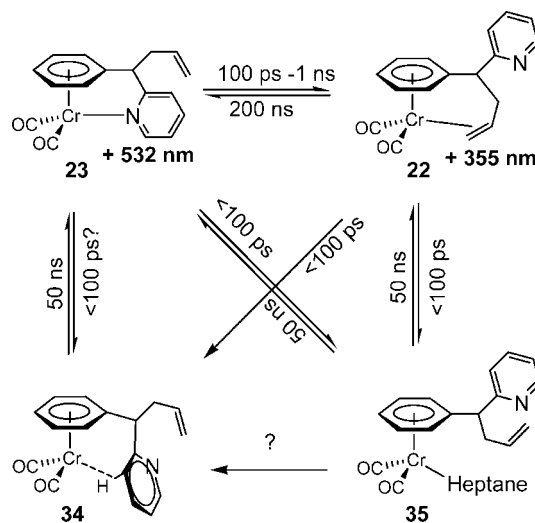
Centennial Feature Article

J. Phys. Chem. A, Vol. 113, No. 12, 2009 **2675**

for the formation of the agostic chelate **30**, which had the shortest tether. Further studies are being designed to examine measures needed to completely eliminate formation of solvent coordinated intermediates and accelerate the linkage isomerization.

Future Directions

The Holy Grail application for photochromic materials is high-speed optical computing and memory.[37] The 50 ns response of the **22/23** photochrome is considerably faster than molecular machines that typically have an upper limit of microseconds.[38] Nevertheless, an analysis of the basic features of the **1/2** photochrome indicate a response near 100 fs could be achieved if excess thermal energy did not produce a significant interference. Faster organometallic photochromes will be designed and prepared with fewer degrees of freedom in their side chains with functional groups that are closer to the metal center. Minimizing fatigue for computing applications will require $>10^{14}$ switching events and is perhaps the most daunting goal. The development of photochromes with near perfect quantum yields or at least near zero side products will be necessary. Though it is important that the quantum yield for interconversion is high in Scheme 2, it is more important that a photon produces only **1** or **2** even if it does not produce the linkage isomerization. Metal−carbonyl bonds will probably be eliminated in more advanced compounds to avoid irreversible dissociation.

Photochromic materials have the ability to store digital information in a single molecule. The information need not be binary because more than two functional groups could be tethered to the metal; although it may be difficult to obtain a spectral change on a single metal center that is large enough to effectively produce more than two distinct chromophores. However, photochromes with two or more different metal centers could be designed. Information density will naturally be limited to the spatial resolution of light beams and will require advances in optical technology (e.g., optical reading and writing).[39]

Less stringent applications would include molecular actuators and nanomachines. Depending on the design of the functional groups, the dimensions of an organometallic photochrome can change during isomerization. The incorporation of a photochrome along the channel of a microfluidic device could act as a light driven gate or peristaltic pump. Photochromes attached near or in the pore of a nanocapsule could eventually be employed to control the flow of reagent in or out of a nanoreactor.[40]

Experimental Section

Spectroscopic Identification Methods.[9] Infrared spectra were obtained with an Analect RFX-75 or a Nicolet 380 Fourier Transform (FTIR) spectrometer, and UV−vis spectra were obtained using an Agilent 8453 UV−vis spectrophotometer.[41] For long timescale interconversion experiments, quasi "steady-state" irradiation was accomplished using excitation pulses from a picosecond Nd:YAG regenerative amplifier at 532 nm (40 ps, 300 μJ/pulse), 355 nm (40 ps, 100 μJ/pulse), or using a Rayonet photochemical reactor (RPR-100) equipped with 300 nm CW xenon lamps (RPR-3000).[41]

Time-Resolved Infrared Spectroscopic Methods. A detailed description of the NIST time-resolved UV-pump infrared probe (TRIR) apparatus used for this study was previously reported.[33,34] In a typical experiment with picosecond time resolution, a 289 nm UV pulse (ca. 120 fs pulse duration with 4−6 μJ energy) was focused to approximately 100 μm diameter in a 2 mm path length flow cell with CaF$_2$ windows. Heptane solutions of **22**

(with UV optical density ca. 0.9 and IR spectral optical densities ca. 0.6) were purged with argon to minimize degradation during photolysis. For experiments requiring higher power 532 and 355 nm excitation pulses (50 ps pulse duration, 40−60 μJ energy), the residual 1.064 μm fundamental pulses after the Nd:YAG regenerative amplifier were frequency doubled with a type I, KDP (potassium dihydrogen phosphate) crystal and then frequency tripled using sum frequency generation (SFG) in KDP type I. For nanosecond to millisecond time resolution, 532 and 355 nm harmonic pulses from a Q-switched Continuum Surelite I Nd:YAG laser[41] (4 ns pulse duration, 40−60 μJ energy), were electronically synchronized and timed to the femtosecond laser system IR probe pulses. To avoid window damage and sample vaporization, the 532 and 355 nm beams were focused to approximately 400 μm diameter in a 2 mm path length flow cell with CaF$_2$ windows. Averages of 2000 laser shots were obtained for a single difference spectrum and two to four of these spectra were averaged for each time delay presented. Analysis of averaged spectra (typically four) yielded an intensity uncertainty from the baseline of less than ± 0.005 optical density (OD) units ($k = 1$; type B analysis). All FTIR photolysis spectra were obtained with a Hg penlamp.

TRIR Sample Preparation. To prepare samples for TRIR experiments, parent Cr complexes (30−50 mg) were dissolved in 50−80 mL of solvent to produce millimolar concentrations (e.g., 1.2×10^{-3} mol/L from 30 mg of **22** in 80 mL of *n*-heptane) with optical density (OD) ~1 measured at the higher CO-stretching frequency (e.g., near 1990 cm^{-1} in heptane) of the doublet CO-stretching peaks. To study the conversion of **22** to **23**, a solution of **23** was subjected to 2 h of 532 nm irradiation, and it was found that 80% (measured by FTIR) of **23** in heptane solution was converted to **22**. The resulting solution was used to obtain TRIR difference spectra for the conversion of **22** to **23**. All samples were studied at room temperature (ca. 293 K) and flowed under positive argon pressure to minimize the possibility of side reactions with air.

Computational Details. The theoretical calculations have been carried out using the Gaussian03[42] implementation of PBE [the PBE exchange functional and correlation functionals[43]] density functional theory[44] with the default pruned fine grids for energies (75, 302), default pruned coarse grids for gradients and Hessians (35, 110) [neither grid is pruned for chromium], and default SCF convergence for geometry optimizations (10^{-8}). All calculations used the same basis set combination. The basis set for chromium (341/341/41) was the Hay and Wadt basis set and effective core potential (ECP) combination (LanL2DZ)[45] as modified by Couty and Hall (341/341/41), where the two outermost p functions have been replaced by a (41) split of the optimized chromium 4p function.[46] All carbons, oxygens, nitrogens, and hydrogens utilized the 6-31G(d′) basis set.[47,48] The density fitting approximation[49] for the fitting of the Coulomb potential was used for all PBE calculations; auxiliary density-fitting basis functions were generated automatically (by the procedure implemented in Gaussian 03) for the specified AO basis set. Spherical harmonic d functions were used throughout; i.e., there are five angular basis functions per d function. All structures were fully optimized, and analytical frequency calculations were performed on all structures to ensure either a minimum or first order saddle point was achieved.

The computational results depicted in Figure 7 are from calculations that have two ethane molecules used to model two solvent molecules (for clarity, only σ-coordinated alkane are shown in Figure 7). For example, in the model utilized to represent **37**, a second ethane is hydrogen bound to the pyridyl

2676 *J. Phys. Chem. A, Vol. 113, No. 12, 2009*

To et al.

nitrogen that is pointed up and away from the metal center. Analogous computations with only one ethane molecule produce energetic and frequency results that are quite similar to those calculations with two ethane molecules. The results presented in Figure 7 with two ethanes are consistent with the results from analogous calculations with one ethane and, when appropriate, no ethane (such as **30** to **TS-30−33** to **33**; **36** to **TS-36−37** to **37**).

Supporting Information Available: Infrared nanosecond kinetic plots and the full citation for ref.[42] This material is available free of charge via the Internet at http://pubs.acs.org.

References and Notes

(1) (a) Dougherty, T. P.; Heilweil, E. J. *Chem. Phys. Lett.* **1994**, *227*, 19–25. (b) Joly, A. G.; Nelson, K. A. *Chem. Phys.* **1991**, *152*, 69–82. (c) Joly, A. G.; Nelson, K. A. *J. Phys. Chem.* **1989**, *93*, 2876–2878. (d) Simon, J. D.; Xie, X. *J. Phys. Chem.* **1987**, *91*, 5538–5540. (e) Simon, J. D.; Xie, X. *J. Phys. Chem.* **1986**, *90*, 6751–6753. (f) Kotz, K. T.; Yang, H.; Snee, P. T.; Payne, C. K.; Harris, C. B. *J. Organomet. Chem.* **2000**, *596*, 183–192. (g) Xie, X.; Simon, J. D. *J. Am. Chem. Soc.* **1990**, *112*, 1130–1136.

(2) Perutz, R. N. *Chem. Soc. Rev.* **1993**, *22*, 361–369.

(3) (a) Brown, C. E.; Ishikawa, Y.-I.; Hackett, P. A.; Rayner, D. M. *J. Am. Chem. Soc.* **1990**, *112*, 2530–2536. (b) Dobson, G. R.; Asali, K.; Cate, C. D.; Cate, C. W. *Inorg. Chem.* **1991**, *30*, 4471–4474. (c) Jiao, T.-J.; Leu, G.-L.; Farrell, G. J.; Burkey, T. J. *J. Am. Chem. Soc.* **1990**, *112*, 4960–4965.

(4) Nasielski, J.; Colas, A. *Inorg. Chem.* **1978**, *17*, 237–240.

(5) Untethered photochromic linkage isomerizations have recently been investigated: Mockus, N. V; Rabinovich, D.; Petersen, J. L; Rack, J. L. *Angew. Chem., Int. Ed.* **2008**, *47*, 1458–1461.

(6) Brown, G. H. *Photochromism*; Wiley: New York, 1971.

(7) Irie, M., Ed. *Chem. Rev.* **2000**, *100*, 1683−1890.

(8) Rachford, A. A.; Petersen, J. L.; Rack, J. L. *Inorg. Chem.* **2006**, *45*, 5953–5960.

(9) Moriuchi, A.; Uchida, K.; Inagaki, A.; Akita, M. *Organometallics* **2005**, *24*, 6382–6392.

(10) El-Sayed, M. A. *J. Phys. Chem.* **1964**, *68*, 433–434.

(11) (a) Geosling, C.; Adamson, A. W.; Gutierrez, A. R. *Inorg. Chim. Acta* **1978**, *29*, 279–287. (b) Mitchell, R. H.; Brkic, Z. S.; Vittorio, A.; Berg, D. J. *J. Am. Chem. Soc.* **2003**, *125*, 7581–7585.

(12) (a) *Organic Photochromic and Thermochromic Compounds*; Crano, J. C., Guglielmetti, R. J., Eds.; Plenum: New York, 1999; Vol. 1 (Main Photochromic Families). (b) Tian, H.; Yang, S. *Chem. Soc. Rev.* **2004**, *33*, 85–97. (c) *Photochromism, Molecules and Systems*; Dürr, H., Bouas-Laurent, H., Eds.; Elsevier: Amsterdam, 2003. (d) Pisignano, D.; Mele, E.; Persano, L.; Athanassiou, A.; Fotakis, C.; Cingolani, R. *J. Phys. Chem. B* **2006**, *110*, 4506–4509.

(13) (a) Zhang, S.; Dobson, G. R. *Organometallics* **1992**, *11*, 2447–2452. (b) Zhang, S.; Dobson, G. R. *Inorg. Chim. Acta* **1989**, *165*, 11–12. (c) Childs, G. I.; Colley, C. S.; Dyer, J.; Grills, D. C.; Sun, X.-Z.; George, M. W., *Dalton Trans.* **2000**, 1901−1906.

(14) Giordano, P. J.; Wrighton, M. S. *Inorg. Chem.* **1977**, *16*, 160–166.

(15) Patterson, M. J.; Hunt, P. A.; Robb, M. A.; Takahasi, O. *J. Phys. Chem. A* **2002**, *102*, 10494–49504.

(16) Yang, H.; Kotz, K. T.; Asplund, M. C.; Wilkens, M. J.; Harris, C. B. *Acc. Chem. Res.* **1999**, *32*, 551–560.

(17) Sorensen, A. A.; Yang, G. K. *J. Am. Chem. Soc.* **1991**, *113*, 7061–7063.

(18) Jiao, T.; Pang, Z.; Burkey, T. J.; Johnston, R. F.; Heimer, T. A.; Kleinman, V. D.; Heilweil, E. J. *J. Am. Chem. Soc.* **1999**, *121*, 4618–4624.

(19) Winnik, M. A. *Chem. Rev.* **1981**, *81*, 491–524.

(20) (a) Schwartz, B. J.; King, J. C.; Zhang, J. K.; Harris, C. B. *Chem. Phys. Lett.* **1993**, *203*, 503–508. (b) Lian, T.; Bromberg, S. E.; Asplund, M. C.; Yang, H.; Harris, C. B. *J. Phys. Chem.* **1996**, *100*, 11994–12001.

(21) Teixeira, G.; Aviles, T.; Dias, A. R.; Pina, F. *J. Organomet. Chem.* **1988**, *353*, 83–91.

(22) Yeston, J. S.; To, T. T.; Burkey, T. J.; Heilweil, E. J. *J. Phys. Chem. B* **2004**, *108*, 4582–4585.

(23) To, T. T.; Heilweil, E. J.; Burkey, T. J. *J. Phys. Chem. A* **2006**, *110*, 10669–10673.

(24) To, T. T.; Barnes, C. E.; Burkey, T. J. *Organometallics* **2004**, *23*, 2708–2714.

(25) To, T. T.; Heilweil, E. J. *J. Phys. Chem. A* **2007**, *111*, 8047–8050.

(26) To, T. T.; Heilweil, E. J.; Duke, C. B., III; Burkey, T. J *J. Phys. Chem. A* **2007**, *111*, 6933–6937.

(27) (a) Wrighton, M. *Chem. Rev.* **1972**, *74*, 401–430. (b) Wrighton, M. S.; Haverty, J. L. *Z. Naturforsch.* **1975**, *30B*, 254–258. (c) Nasielski, J.; Denishoff, O. *J. Organomet. Chem.* **1975**, *102*, 65–70. (d) Hu, S.; Burkey, T. J. Unpublished result in heptane.

(28) To, T. T.; Duke, C. B., III; Junker, C. S.; O'Brien, C.; Ross, C. R., II; Barnes, C. E.; Webster, C. E.; Burkey, T. J. *Organometallics* **2008**, *27*, 289–296.

(29) To, T. T.; Barnes, C. E.; Burkey, T. J. *Organometallics* **2004**, *23*, 2708–2714.

(30) Rybinskaya, M. I.; Korneva, L. M. *J. Organomet. Chem.* **1982**, *231*, 25–35.

(31) Duke, B. C., III; Ross, C. R., II; Burkey, T. J. *Organometallics*, manuscript in preparation.

(32) Creaven, B. S.; George, M. W.; Ginzburg, A. G.; Hughes, C.; Kelly, J. M.; Long, C.; McGrath, I. M.; Pryce, M. T. *Organometallics* **1993**, *12*, 3127–3131.

(33) (a) To, T. T; Duke, B. C., III; Burkey, T. J.; Heilweil, E. J. *J. Phys. Chem. A* **2007**, *111*, 6933–6937. (b) To, T. T; Burkey, T. J.; Heilweil, E. J. *J. Phys. Chem. A* **2006**, *110*, 10669–10673. (c) Yeston, J. S.; To, T. T; Burkey, T. J.; Heilweil, E. J. *J. Phys. Chem. B* **2004**, *108*, 4582–4585.

(34) Jiao, T.; Pang, Z.; Burkey, T. J.; Johnston, R. F.; Heimer, T. A.; Kleiman, V. D.; Heilweil, E. J. *J. Am. Chem. Soc.* **1999**, *121*, 4618–4624.

(35) We attempted to computationally locate an η^2-bound pyridyl geometry for a structure similar to **30**. Though we have previously located η^2-π-bound pyridyl geometry for a related photochromic (CpR)Mn(CO)$_2$ complex,[28] there is not an η^2-π-bound pyridyl local minimum (stationary point on the potential energy surface) for this Cr system.

(36) This solution is prepared by 532 nm irradiation, converting 80% to 90% of **23** to **22** in *n*-heptane as monitored by FTIR.

(37) Frigoli, M.; Mehl, G. H. *Proc. SPIE Int. Soc. Opt. Eng.* **2004**, *5289*, 1–7.

(38) Balzani, V.; Credi, A.; Ferrer, B.; Silvi, S.; Venturi, M. *Top. Curr. Chem.* **2005**, *262*, 1–27.

(39) Kling, James. *R&D Mag.* **1996**, *38*, 46–47.

(40) Dergunov, S. A.; Pinkhassik, E. *Angew. Chem., Int. Ed.* **2008**, *47*, 8264–8267.

(41) Certain commercial equipment, instruments, or materials are identified in this paper to adequately specify the experimental procedure. In no case does such identification imply recommendation or endorsement by NIST, nor does it imply that the materials or equipment identified are necessarily the best available for the purpose.

(42) Frisch, M. J. *Gaussian 03*, revisions C.02; Gaussian, Inc.: Wallingford, CT, 2004.

(43) (a) Perdew, J. P.; Burke, K.; Ernzerhof, M. *Phys. Rev. Lett.* **1996**, *77*, 3865–3868. (b) Erratum *Phys. Rev. Lett.* **1997**, *78*, 1396.

(44) Parr, R. G.; Yang, W. *Density Functional Theory of Atoms and Molecules*; Oxford University Press: New York, 1989.

(45) (a) Hay, P. J.; Wadt, W. R. *J. Chem. Phys.* **1985**, *82*, 270–283. (b) Wadt, W. R.; Hay, P. J. *J. Chem. Phys.* **1985**, *82*, 284–298.

(46) Couty, M.; Hall, M. B. *J. Comput. Chem.* **1996**, *17*, 1359–1370.

(47) Hariharan, P. C.; Pople, J. A. *Theor. Chim Acta* **1973**, *28*, 213–222.

(48) The 6-31G(d′) basis set has the exponent for the d polarization function for C, O, and N taken from the 6-311G(d) basis sets, instead of the original arbitrarily assigned value of 0.8 used in the 6-31G(d) basis sets.

(49) (a) Dunlap, B. I.; Connolly, J. W. D.; Sabin, J. R. *J. Chem. Phys.* **1979**, *71*, 3396–3402. (b) Dunlap, B. I.; Connolly, J. W. D.; Sabin, J. R. *J. Chem. Phys.* **1979**, *71*, 4993–4999. (c) Dunlap, B. I. *J. Chem. Phys.* **1983**, *78*, 3140–3142. (d) Dunlap, B. I. *J. Mol. Struct. (THEOCHEM)* **2000**, *529*, 37–40.